Improved Contrast of Peripapillary Hyperpigmentation Using Polarization Analysis

Mariane B. Mellem-Kairala,[1,2] *Ann E. Elsner,*[1] *Anke Weber,*[1,3] *Ruthanne B. Simmons,*[4,5] *and Stephen A. Burns*[1]

Purpose. To improve detection and quantification of peripapillary hyperpigmentation, associated with aging, open-angle glaucoma, and age-related macular degeneration.

Methods. A computational approach was implemented with a readily available polarimeter used in glaucoma diagnosis, a nerve fiber analyzer (GDx; Laser Diagnostic Technologies, San Diego, CA). Using near-infrared illumination at each of 20 input polarizations, a series of image pairs was digitized. One image is made from the light returning from the eye that is polarized parallel to the input light, and the other image is made from the light that is rotated by 90° from the input polarization. Using raw data from these 40 images, and a simplified model of ocular polarization properties, images were computed based on their polarization content. Regions of hyperpigmentation, selected using stereo color fundus photographs, were quantified in three types of polarimetry images: (1) a depolarized light image resulting mainly from multiply scattered light; (2) an average image that is typical of confocal images; and (3) a birefringence image. Measurements on versus off hyperpigmentation were made in nine persons with suspected glaucoma or patients with primary open-angle glaucoma, selected to have clinically visible hyperpigmentation.

Results. In the depolarized light images, hyperpigmented regions were significantly brighter than comparison areas ($P < 0.0425$)—that is, had more scattered light and therefore more contrast ($P < 0.037$) than did color or other polarimetric images.

Conclusions. With this polarimetry imaging method, subretinal tissues such as those with hyperpigmentation can be visualized with increased contrast. (*Invest Ophthalmol Vis Sci.* 2005;46:1099–1106) DOI:10.1167/iovs.04-0574

The pathophysiology of glaucoma, one of the leading causes of blindness in the world, is not yet fully understood because of the multifactorial nature of the disease.[1] However, it is well known that the progression of glaucoma leads to morphologic changes in the optic disc and peripapillary region. The occurrence of peripapillary chorioretinal atrophy and hyperpigmentation has been described in patients with chronic open-angle glaucoma.[2,3] The presence of these peripapillary changes, and moreover the change over time, is helpful in differentiating between glaucomatous and nonglaucomatous optic nerve damage or to rule out glaucomalike discs.[4,5] Moreover, several studies have shown that peripapillary atrophy and hyperpigmentation are useful in the classification and differentiation of open-angle glaucoma, since their presence occurs more frequently in some types of glaucoma than in others.[6–8]

The present study was performed to investigate further the peripapillary abnormalities in patients with glaucoma by using a new imaging method based on polarimetry, described previously.[9,10] Hyperpigmentation has been identified in many eyes preceding the development of geographic atrophy in the macular region, and these areas of hyperpigmentation indicate areas of diseased retinal pigment epithelium (RPE) at extreme risk.[11] In both the macular and peripapillary regions, these pigmentary changes correspond histologically to degenerating RPE cells of nonuniform size and melanin content. These changes simultaneously occur with changes to photoreceptors, Bruch's membrane, and the choriocapillaris.[11,12] Older adult eyes typically show some peripapillary pigmentary changes.[13] Pigmentary changes are not routinely studied as a predictive factor for the progression of glaucoma, but their presence indicates degeneration of the RPE-Bruch's membrane complex surrounding the optic nerve head. The lack of a sensitive method that is immune to the normal variation of fundus pigmentation is needed before peripapillary changes can be fully tested as a reliable predictive factor across individuals and disease stages.

Pigmentary changes can be seen in indirect ophthalmoscopy and color fundus photographs. We investigated whether our polarimetric imaging method would reveal tissue disorder in the peripapillary region, to a greater extent than do standard methods. In advanced glaucoma, deeper structures such as hyperpigmentation may be visualized not only because they appear with more severe damage but also because they show through the thinned nerve fiber layer. For early detection, and for progression, a method is needed that reduces the contribution of the nerve fiber layer so that the deeper structures are revealed.

We have shown that polarization analysis offers the opportunity to emphasize different layers or features of the fundus selectively in retinal images.[9,10] Information about the nerve fiber layer and superficial structures such as blood vessel walls are obtained in images by using light that is polarization preserving. The deeper structures can be emphasized by removing

From the [1]Schepens Eye Research Institute and Harvard Medical School, Boston, Massachusetts; the [2]Department of Ophthalmology, Ribeirão Preto Medical School, University of São Paulo, São Paulo, Brazil; the [3]Ophthalmic Consultants of Boston, Boston, Massachusetts; and the [4]Department of Ophthalmology, University Hospital, Rheinisch-Westfälisch Technische Hochschule, Aachen, Germany.

[5]Deceased November 8, 2002.

Presented in part at the annual meeting of the Association for Research in Vision and Ophthalmology, Fort Lauderdale, Florida, May 2002.

Supported by National Eye Institute Grant EY07624 and the Richard Saltonstall Foundation (AEE).

This technology is specifically not funded by the Small Business Innovative Research grant with Laser Diagnostic Technologies. They choose not to license it at this time. The authors are permitted but not obligated to seek other licensees.

Submitted for publication May 21, 2004; revised October 18, 2004; accepted November 22, 2004.

Disclosure: **M.B. Mellem-Kairala**, None; **A.E. Elsner** (P); **A. Weber**, None; **R.B. Simmons**, None; **S.A. Burns** (P)

The publication costs of this article were defrayed in part by page charge payment. This article must therefore be marked "*advertisement*" in accordance with 18 U.S.C. §1734 solely to indicate this fact.

Corresponding author: Ann E. Elsner, Schepens Eye Research Institute, Harvard Medical School, 20 Staniford Street, Boston, MA 02114; elsner@vision.eri.harvard.edu.

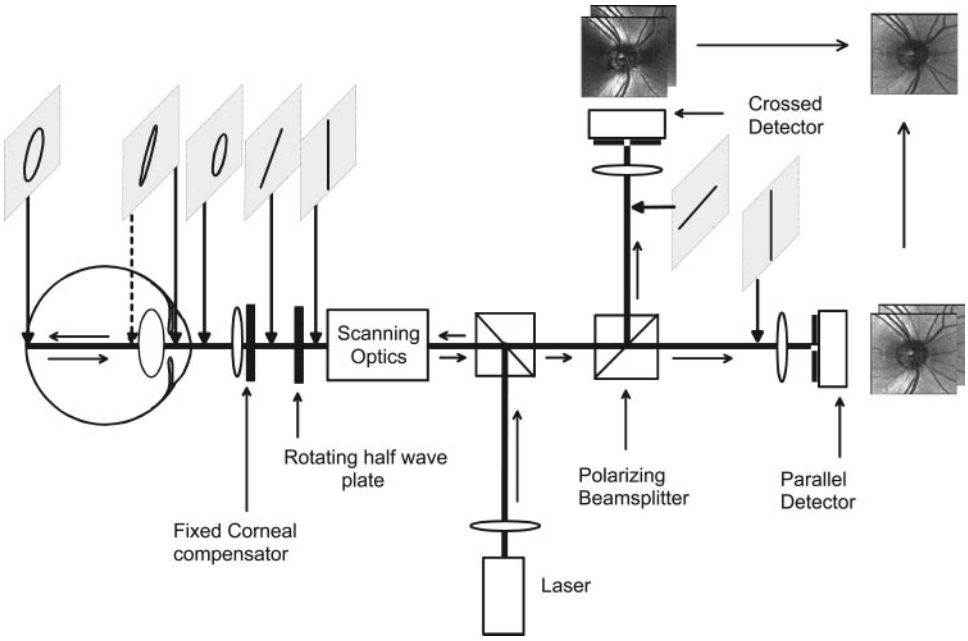

FIGURE 1. Schematic diagram of the scanning laser polarimeter and computation of images. The *shaded boxes* show the effect of the optical elements of the apparatus and the eye, in one plane and as a snapshot. Linearly polarized light, shown in the *shaded box* above the scanning optics, is rotated by the half-wave plate to provide 20 different input polarizations, as shown in the *shaded box* after the half-wave plate. A fixed corneal compensator leads to somewhat elliptically polarized light, shown in the corresponding *shaded box*. The human cornea, on average, produces less elliptically polarized light, as shown by the *shaded box* above the anterior segment of the eye. The lens has little effect, indicated by a *dotted line*, unless there is significant scatter that leads to phenomena such as depolarization. The first pass through the retina leads to at least some retardance, as indicated in the *shaded box* above the posterior segment. Then, the light travels back through the same optical elements, with similar effects expected, until reaching the polarizing beam splitter, where it is split into two beams. The light passes through the detector for uncrossed polarization and a detector for crossed polarization. Light reaching the two detectors is digitized pair-wise for a series of input polarization angles. The 40 total raw images from both detectors are used to compute different types of images, according to their polarization content, with a depolarized light image shown at the *top right*.

this polarization preserving light. Then, the remaining light, which has passed through the retina and been multiply scattered, forms a useful and novel image.[14–17] However, most previous multiply scattered light imaging studies have relied on techniques with annular or displaced apertures. Multiply scattered light images show enhanced contrast of drusen, which are in the layers beneath the retina,[9,10,14–17] and we now extend the polarimetry method to another subretinal feature: hyperpigmentation.

Our hypothesis is that changes in polarization properties of the peripapillary region may help to classify disease state and track progression, by being more resistant to contrast variation arising from various amounts of nerve fiber layer loss. Specifically, although focal hyperpigmentation often appears dark due to increased absorption of concentrated melanin and debris, we anticipate that the focal disruption of the tissues leads to increased scattered light and to increased brightness of these tissues in scattered light images when compared to surrounding tissue. However, when the disease is not focal and is embedded in a larger region of diverse disease, the index of refraction changes may require a much more detailed model. Thus, to test our hypothesis, we confined our sample to focal hyperpigmentation in patients without widespread atrophy.

SUBJECTS AND METHODS

We performed a cross-sectional study using a commercial infrared scanning laser polarimeter in 10 eyes of 10 patients (6 women, 4 men; mean age, 56 years). The patients were selected by a glaucoma specialist (RBS) for having peripapillary atrophy (PPA) and/or pigmentary changes (PPP) in one or both eyes. The patients enrolled in this study either presented with manifest primary open-angle glaucoma or had suspected glaucoma. IOP was <25 mm Hg, controlled by topical treatment when necessary. Visual acuity was 20/60 or better, with ametropia <6 D. Patients with previous eye trauma, other severe eye diseases such as diabetic retinopathy or age-related macular degeneration (AMD), or previous ocular surgery other than cataract extraction were deemed ineligible. All patients underwent a complete ophthalmic examination by two glaucoma specialists, including visual acuity, slit lamp biomicroscopy, and indirect ophthalmoscopy. Intraocular pressure was measured by a trained technician in a standardized manner with a slit lamp mounted applanation tonometer. Automated perimetry using the 24-2 program was applied with the full-threshold strategy (Humphrey Visual Field Analyzer; Carl Zeiss Meditec, Dublin, CA), and 30° color fundus photographs were obtained. The research followed the tenets of the Declaration of Helsinki. Informed consent was obtained from the subjects after explanation of the nature and possible consequences of the study. The research was approved by the Institutional Review Board of the Schepens Eye Research Institute.

Scanning laser polarimetry was performed in all patients (GDx; Laser Diagnostic Technologies, San Diego, CA). This device was originally developed to measure the thickness of the nerve fiber layer by birefringence.[18] The instrument is designed to be used with pupils of only 2.5 mm in diameter—that is, having an entrance and exit pupil of 2.5 mm. As only 2 mW of near-infrared light (780 nm) is present at the cornea, the light level is comfortable. When lens changes are present, this wavelength more readily penetrates to visualize the retinal and subretinal structures than does short-wavelength light. Figure 1 shows a schematic of the system. Linearly polarized light is rotated by a half-wave plate to 20 different input polarization angles. For each of these angles, the retina is scanned in a raster pattern of 15° × 15° visual angle. The returning light is passed back through all the same optical elements as the illumination pathway, until reaching a polarizing beam splitter. There, the light is split into two beams, one of the same polarization as the illumination light (parallel polarized light, i.e., the detector for uncrossed polarization) and the other that collects light polarized at 90° to the illumination light (the detector for crossed polarization). Each beam passes through a small confocal aperture and is focused on an avalanche photodiode detector. In <1 second, 20 pairs of images are digitized from the amplitude signals of the detectors, with one image per detector and each pair representing illumination with a different angle of polarization for the illumination light. Each image of a series is saved as 256 × 256 pixels with 8 bits of gray scale. The polarization properties of the entire human eye, and not just the retinal and subretinal tissues, must be considered in the interpretation of these images, as noted in Figure 1 and the Discussion section.

Infrared confocal scanning laser polarimetry was performed without pupil dilation at the Ophthalmic Consultants of Boston by an experienced operator. For each eye, image series were obtained and then the raw data, which are typically not available, were saved to hard disk.

Raw data were processed from the GDx image series to generate images based on the polarization content of the returning light, and some of these do not exist as instrument output and are available only as computed images. We developed a set of computer routines (MatLab; The MathWorks, Natick, MA) to generate these images from the raw images.[9,10] As for other analysis with this type of imaging, the best computations are obtained from properly focused image series with a centrally located optic disc, minimal eye movement artifact, and equal illumination in all quadrants. In our analysis, we assume that the changes in the measurable polarization properties are either due to the birefringence of the cornea and retinal nerve fiber layer or to multiple scattering in the retina and RPE. The cornea and to a lesser extent the lens are birefringent elements unrelated to the comparisons of interest in the current studies. Their effects were minimized by a fixed corneal compensator. The isolation per se of the depolarized light component can be decreased with incorrect compensation of corneal polarization. The influence of uncompensated birefringence is not critical for our purposes. This potential artifact causes an underestimation of the improvement in this type of imaging, and the expected decrease in improvement is small.[10]

All images were aligned to correct for eye movements. Next, we computed the following three image types (Fig. 2A–D): (1) a depolarized light image, computed as the minimum value of light returning to the detector for crossed polarization at each pixel for all input polarization angles; (2) an average image of all the light returning to both detectors for all the input polarization angles; and (3) a birefringence image, which represents the modulation of amplitude of light returning to the detector for crossed polarization. The average image is similar to near-infrared scanning laser images collected with small, confocal apertures.[19,20]

The color fundus photographs were digitized at 2000 dpi and up to 12 bits per channel (SprintScan 4000; Polaroid, Cambridge, MA). Using the stereo optic disc photographs (VRex, Hauphauge, NY), one of the investigators (MBMK) manually outlined the border of the disc rim and marked the areas of the hyperpigmentation for each patient, as shown in Figure 2E (Photoshop; Adobe, San Jose, CA). We considered the peripapillary region within a 2° (600 μm) width from the disc rim, and hyperpigmentation was sampled only within this area. Pixels were converted into square micrometers. A template was placed over the optic nerve head to determine the four different segments: nasal, temporal, superior, and inferior. The GDx template divides the peripapillary region into unequal segments, with the nasal segment at $\pm$35° from the horizontal, the temporal at $\pm$25° from horizontal, and the superior and inferior segments covering the remaining areas. Hyperpigmentation was graded in one of the following three different stages: 1, minimal pigmentary changes; 2, intermediate pigmentary changes; and 3, clumped pigment, as previously graded for patients with age-related macular degeneration.[21]

On examination of the fundus photographs, peripapillary hyperpigmentation appeared dark, as expected, but it appeared bright in the computed depolarized light image, as hypothesized, due to increased scattering. This finding was taken into account for the following analysis. A 3 $\times$ 3-pixel region was selected in a region of interest containing the hyperpigmentation in each computed polarimetry image, and average gray-scale values were calculated on computer (MatLab; The MathWorks; Fig. 2F). The same calculation was made for a control region (3 $\times$ 3 pixels) located approximately 200 μm away from the hyperpigmentation.

The color fundus photographs were manually aligned to the computed polarimetry images to have the same magnification as the computed images (Photoshop; Adobe) and were split into the three different color channels: red, green, and blue. The areas corresponding to those in the computed images were marked on the three different color images, and average intensities were calculated by using histograms in the image-management program. The sizes of the regions of interests for the color photographs and polarimetry images were the same, regardless of the number of pixels and the differing resolutions.

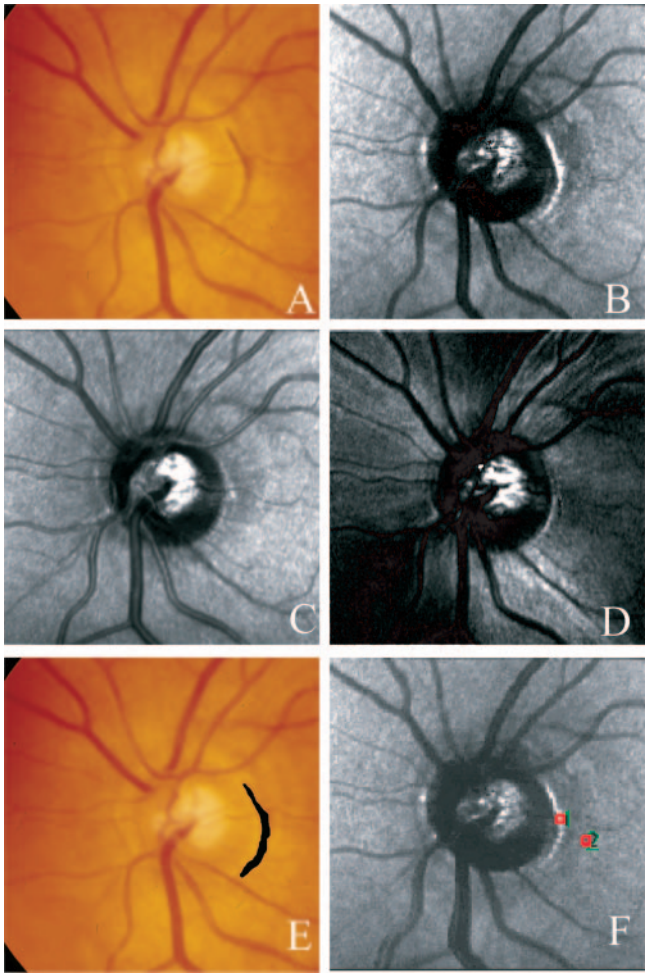

FIGURE 2. Comparison of polarimetry images and color fundus photographs, showing peripapillary hyperpigmentation of the optic nerve head of the left eye of patient 8. (**A**) Color fundus photograph. (**B**) The depolarized light image with hyperpigmented regions shown as bright. Note that blood vessels appear wide and lack the striped appearance of typical confocal images, and the superficial retinal features are diminished in contrast. The neuroretinal rim of the optic nerve head appears dark since, typically, the light returning from this area scatters within the volume of the optic nerve head and is blocked by the aperture, whereas the excavation appears light. (**C**) Average image, showing the hyperpigmentation as dark. The retinal vessels have the typical striped appearance found in confocal images. The choroidal rim of the optic nerve head is somewhat obscured by the superficial retinal features, despite thinning of the retinal nerve fiber layer due to glaucoma. (**D**) The birefringence image, showing some superficial retinal features and that the contribution to polarization retaining images is dominated by the nerve fiber layer and other reflective structures. (**E**) Manually marked hyperpigmentation in the color fundus photograph. (**F**) Depolarized light image with 3 $\times$ 3-pixel boxes set on hyperpigmentation and on a control area.

From the averaged gray-scale values for each polarimetry image and the three channels for the color fundus photographs, we calculated the difference for on versus off hyperpigmentation by using the Michelson contrast. The Michelson contrast is a metric that helps to decrease the influence of variations in illumination or fundus pigmentation. Michelson contrast is defined as $MC = (I_{feature} - I_{adjacent})/(I_{feature} + I_{adjacent})$, where $I_{feature}$ is the average gray-scale value of the hyperpigmentation

TABLE 1. Demographic Data, Clinical Data, Peripapillary Grading, and Hyperpigmention Area in the Study Patients

Case	Age	Eye	Sex	RE*	IOP†	Diagnosis	HVF‡	PPP Grade‖	Hyperpigmentation (μm^2)
1	45	OD	F	Plano	16	GS	Normal	3	1598.87
2	46	OS	F	Plano	12	GS	Normal	3	8837.71
3	48	OD	M	Plano	16	GS	Normal	3	5921.09
4	59	OD	M	−4.00	18	GS	Normal	2	1774.57
5	61	OS	M	1.25	16	GS	Normal	2	1862.42
6	61	OS	M	Plano	17	GS	Inferior nonspecific defects	3	14442.54
7	59	OD	F	Plano	10	POAG	Superior arcuate scotoma/forming inferiorly	3	59667.72
8	59	OS	F	0.75	18	POAG	Superior nasal step + superior defects	3	8591.73
9	61	OS	F	Plano	14	POAG	Paracentral scotoma	3	790.65
10	63	OD	F	−1.00	11	POAG	Superior arcuate scotoma, not closed	3	2090.83

* Refractive Error.
† Intraocular pressure.
‡ Humphrey Visual Field.
‖ Peripapillary pigmentation grade.

region of interest and $I_{adjacent}$ of the region of interest approximately 200 μm away.

Statistical analysis included paired *t*-tests for the mean gray-scale and the resultant Michelson contrast, comparing on versus off hyperpigmentation in each channel of the color photographs, as well as in each of the three computed polarimetry images (StatView; Abacus Concepts, Berkeley, CA). We additionally compared the Michelson contrast for on versus off hyperpigmentation for the depolarized light images and the blue channel images.

RESULTS

Hyperpigmentation was readily visualized with polarimetric analysis, even when it was subtle, in the patients in our study. Of the 10 initially enrolled patients with clinically visible hyperpigmentation, four had manifest open-angle glaucoma with typical visual field loss, whereas only one of the six with suspected glaucoma had visual field loss. For further demographic information, refractive error, IOP, diagnosis, type of visual field loss, hyperpigmentation grade, and area of hyperpigmentation within the sampled region, see Table 1. One patient (case 7) was excluded from all statistical analysis because of the extensiveness of the area containing peripapillary atrophy and hyperpigmentation, >50,000 μm^2. Not only the size but also the irregularity of pigment in the color fundus photograph might diminish objectivity (Fig. 3A).

All the computed images provided detail for the subretinal structures, even for the excluded patient. The algorithm to compute depolarized light images successfully reduced specular reflections. For instance, there was a lack of vessel wall reflections for the major retinal vessel in all patients, as shown by comparing the depolarized light image in Figure 2B with its corresponding randomly polarized light image in Figure 2C. This contrast is also shown in Figures 3B compared with 3C. The blood vessels have a dark appearance, and we have already shown that the intensity profile has no corresponding irregularity of the type that is typical of vessel wall reflections.[9,22] Figures 3B–D show that the depolarized light image has clear-cut peripapillary features and good detail over the whole figure, despite that the birefringence image indicates the loss of nerve fiber in specific locations.[18] That is, the depolarized light image was not degraded by long-range scatter from the extensive atrophic region, nor was it of uneven intensity, despite the unevenness of the nerve fiber layer, as revealed in the birefringence image.

The average mean differences of the gray-scales for on versus off hyperpigmentation for the three computed images were 6.71 ± 8.36, 5.55 ± 8.68, and 1.73 ± 19.41 for the depolarized light image, the average image, and the birefringence image, respectively. The areas of hyperpigmentation appeared focal and corresponded to the locations seen in the color fundus photographs, indicating that there was good separation of multiply scattered light from retinal layers compared with long-range scatter from anterior segment artifact.

The gray-scale values for on versus off hyperpigmentation were significantly different only in the depolarized images (P =

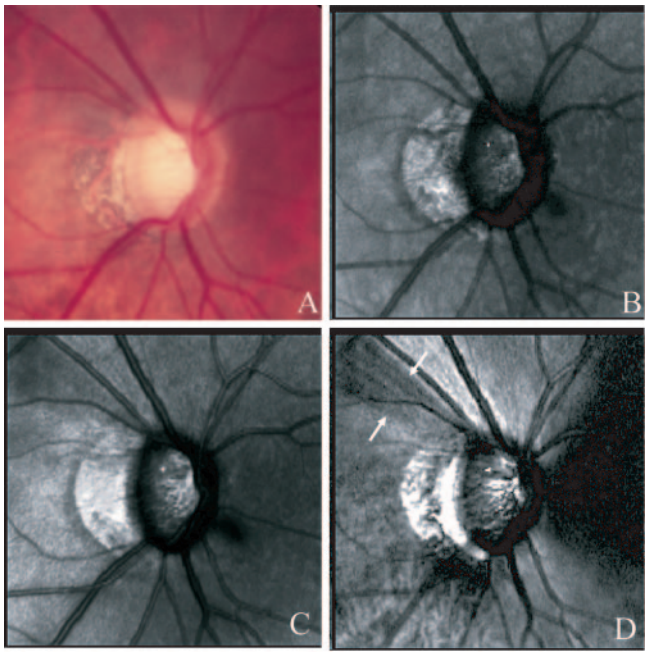

FIGURE 3. Comparison of polarimetry images and color fundus photographs, showing extensive peripapillary hyperpigmentation and atrophy of the optic nerve head of the right eye of patient 7. (**A**) Color fundus photograph, showing hypo- and hyperpigmented regions, often in proximity and with unclear borders. Choroidal vessels are well visualized. (**B**) The depolarized light image, demonstrating a large, bright area of peripapillary atrophy with clear borders, but less distinct choroidal vessels showing through. (**C**) Average image, showing the atrophic area as bright, but poorly showing the choroidal vessels and pigmentary changes. (**D**) The birefringence image, showing some superficial retinal features and deeper features where the retina is extremely thinned. The contribution of polarization-retaining images is dominated by the nerve fiber layer, which is brightest in the superior and inferior segments, darker temporally and nasally. *White arrows*: a fiber bundle defect, appearing as a darker radial region at 11 o'clock.

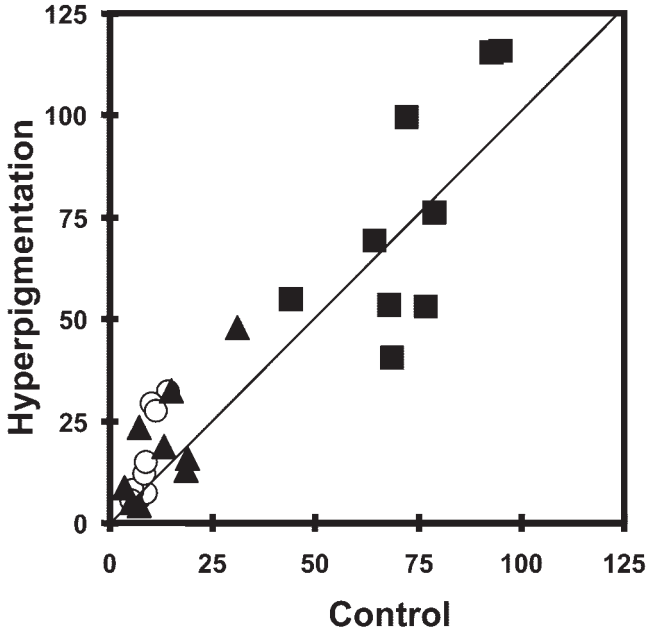

FIGURE 4. Comparison of gray-scale values on versus off hyperpigmentation. (○) Depolarized image; (■) average image; and (▲) birefringence image.

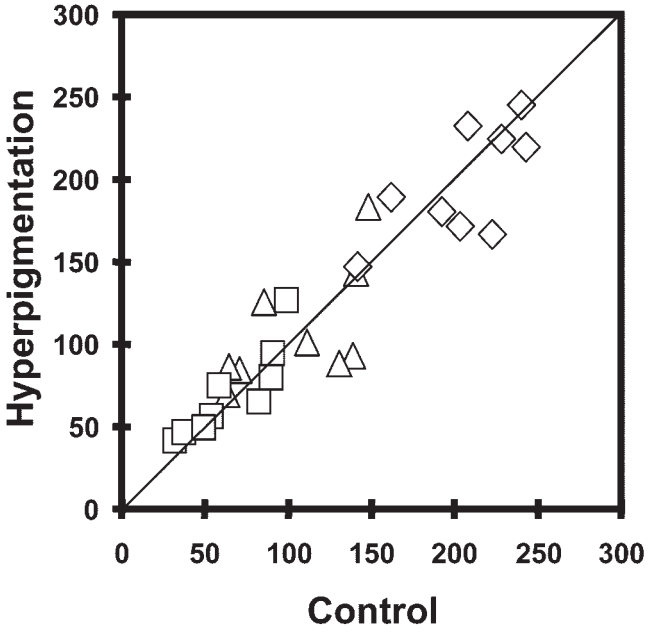

FIGURE 5. Comparison of the average intensities for the red, green, and blue channels of the color fundus photographs. (□) Blue, (△) green, and (◇) red channels.

0.0425) and not in the average images ($P = 0.807$) or the birefringence images ($P = 0.108$; Fig. 4). Similarly, Michelson contrasts were significantly different for the comparison of on versus off hyperpigmentation in depolarized images ($P = 0.037$), but lacked statistical significance for the other computed images ($P = 0.189$ for the birefringence image; $P = 0.865$ for the average image).

The average intensities sampled in our images for the separated color channels did not differ significantly for on versus off hyperpigmentation ($P = 0.83$ for the green channel, $P = 0.42$ for the red channel, and $P = 0.39$ for the blue channel). Figure 5 shows that the hyperpigmentation sample was often similar to the control sample, and, when these differed, it was not in a consistent direction. Thus, the intensity of each channel separately did not lead to statistically different values, although a human observer might see the two regions as different colors. Similarly, Michelson contrasts were also not statistically significant for the green ($P = 0.74$), the red ($P = 0.45$), or the blue ($P = 0.29$) channel images for on versus off hyperpigmentation.

Figure 6 shows the Michelson contrasts for the depolarized light images, which are positive, except for those of subjects 3, 4, and 7, and of generally larger absolute value compared with those of the average images or the blue channel of the color fundus photographs. The red and green channels were even more variable and thus are not shown. It could be the case that a human observer could detect a difference in either color or brightness, whereas the computer could not.

The mean area of hyperpigmentation, as measured in the color photographs was 2.15% ± 1.96% of the sampled peripapillary region. The total area of the hyperpigmentation in each quadrant was as follows: temporal quadrant, 162 ± 154 μm^2 (46%); superior quadrant, 59 ± 149 μm^2 (30%); inferior quadrant, 88 ± 101 μm^2 (24%); and nasal quadrant, 0 μm^2 (0%).

DISCUSSION

We used a novel method of analysis for polarimetry data, intentionally computing images that visualized scattered light primarily from deeper structures in the fundus. In keeping with the hypothesis that the scattered light would dominate other optical phenomena in the depolarized light images,[10] the regions of hyperpigmentation in depolarized light images were bright, rather than having the more traditional dark appearance.[14–16] The average images that corresponded to typical confocal, near-infrared images visualized the hyperpigmentation typically as dark, but provided less contrast. The birefringence images often showed little contrast for hyperpigmentation, as expected, because it lies beneath the nerve fiber layer. Although the nerve fiber layer was probably thinned in these patients, reflected light from the nerve fiber layer nevertheless dominated those images computed from light that retained polarization, as previously known from tomographic measurements in glaucoma diagnosis.[19,23,24]

The goal of this imaging method is to visualize small, pathologic features at high contrast, rather than to provide informa-

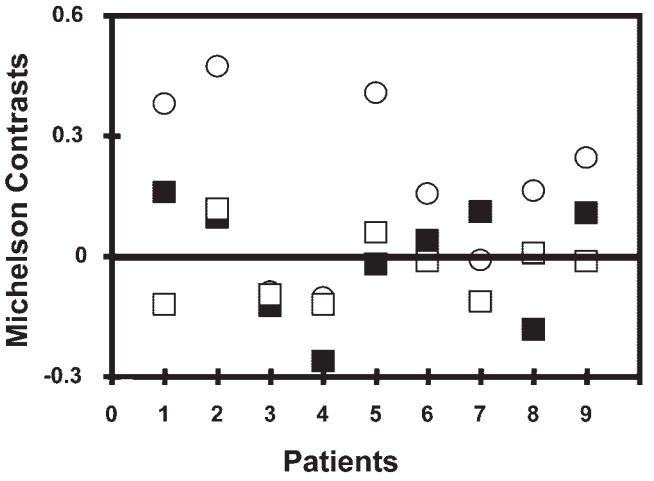

FIGURE 6. Michelson contrasts for each patient. (○) Depolarized image; (■) average images; and (□) blue channel.

tion about layers of tissues, such as numerical estimates of thickness.[18] Scattered light, whether due to atrophy or hyperpigmentation, is visualized as bright by our depolarized images. This could be an advantage in that a region with several bright areas may be more recognizable as abnormal than would a few discrete, focal areas of hyperpigmentation. In grading studies and clinical examination of AMD, hyperpigmentation and hypopigmentation are often combined into the single category of "pigmentary changes."[25] However, the appearance of specific pathologic features may differ between the polarimetry method used in this study and previously used methods, involving annular confocal apertures and also longer or shorter wavelengths[11,15] or lateral displacement of the aperture with respect to the illumination.[17] Further, most previous images were collected with larger-diameter apertures, allowing more and longer range scattered light and less sectioning of layers, consequently losing spatial resolution while delineating the large scattering structures. Additional clinical experience with polarimetry may be necessary before its utility for macular disease can be assessed.

The depolarized light images visualized regions of hyperpigmentation with higher contrast than any of the three channels of the color fundus photographs. Sometimes the control regions of interest were not brighter than the focal regions of hyperpigmentation, because of typical variations in fundus pigmentation across the retina, and this experimental difficulty occurred more frequently for the color fundus photographs than for the depolarized light images. Although the color fundus photographs were collected at higher spatial resolution and increased sampling can often improve signal-to-noise ratio, this increased sample size per pixel and consequently larger data file size had fewer, not more, statistically significant results. Models of combining color information across differently pigmented fundi do not yet exist for hyperpigmentation, and therefore the combination of three channels was not tested. However, there is an inherent difficulty with the fundus photography method, in that the nerve fiber layer can obscure peripapillary hyperpigmentation in normal subjects, whereas thinning of the nerve fiber layer allows the peripapillary hyperpigmentation to be revealed. Thus, the relation between the nerve fiber layer and RPE and photoreceptor loss was concluded to be unclear with this method.[12]

The pattern of hyperpigmentation that could be quantified in the color fundus images of our patients indicates two things. First, after removal of the patient with the more advanced peripapillary atrophy and hyperpigmentation, we had a patient sample with small, often multiple, regions of hyperpigmentation. We did not need a large sample size to obtain significant differences between depolarized light images and all three color separation images. With large lesions of the type we omitted, the pathologic tissues are typically even more visible. Second, our technique works on small regions of hyperpigmentation that were specifically sought by an experienced clinician, but that might in some cases be missed. Thus, the polarimetry technique provides more contrast and can be used on small regions. We tested only patients who still had sufficiently clear media that hyperpigmentation could be detected on clinical examination and with color fundus photographs. Confocal, near infrared imaging has already been shown to have the advantages of penetrating through cataract, providing a useful image in darkly pigmented fundi, and reducing long-range scatter from a variety of ocular media changes.[14] This type of instrument does not require the pupil dilatation that is necessary for the high-quality fundus photographs, and the light levels are safe and comfortable.

The polarimetry imaging method seems suited for early detection of hyperpigmentation, either in new patients or as a potential means to determine progression of peripapillary damage. Chorioretinal abnormalities, such as atrophy or hyperpigmentation, have been reported to occur in some but not all eyes with glaucomatous optic nerve damage. Ophthalmoscopically, these changes have been divided into a central beta zone and a more peripheral alpha zone. The beta zone shows visible sclera, due to a complete loss of the RPE cells and a decreased number of photoreceptors, whereas the alpha zone is characterized by uneven hypo- and hyperpigmentation that histologically correspond to pigmentary irregularities in the RPE.[13,26–28]

Pigmentary changes, such as hyperpigmentation, result from severe damage to the RPE layer, and therefore may be an important sign of disease related damage to deeper layers of the retina.[11,12,16] This may occur, not only in glaucoma but also in other diseases that affect the RPE, particularly when the RPE is one of the primary sites, such as in AMD. For AMD, focal hyperpigmentation is a well-known risk factor for disease progression.[11,29–31] It is not known whether these changes are a very early sign of damage or merely quite visible, particularly once the retina is thinned.

Our novel polarimetry method has been shown to lead to enhanced contrast of subretinal features such as drusen.[10] We have shown that it will also provide information for the hyperpigmented regions around the optic nerve head. Polarimetry methods have evolved[32] so that they now distinguish the polarization retaining light from the depolarized light.[9,10,33] We intentionally compute images that visualize features in scattered light, primarily originating from deeper structures in the fundus. This is one key difference between our method and the wide variety of new polarimetry methods that are optimized for high contrast[34] or light with scatter minimized to the extent that a coherence method can be used[35]—that is, polarization retaining light.

The present results support our previous findings that different features are emphasized according to the proportion of polarization retaining light in the image, with superficial features better visualized with a high proportion of polarization containing light and deeper features visualized better for images that diminish the proportion of polarization retaining light.[9,10,33] For glaucoma management, several important features were rapidly visualized in a few key computed images, without the need for dilatation or uncomfortably bright light. These features include the optic nerve head rim and cup, pores in the lamina cribrosa, a nerve bundle defect, peripapillary hyperpigmentation, peripapillary atrophy, retinal arteries and veins, the arterioles and veins associated with the optic nerve head, and the distribution of birefringence associated with the measurement of retinal nerve fiber layer thickness. In addition to visualizing features, the depolarized light images have been used to obtain better information from beneath and within blood vessels, because the specular reflection from blood vessel surfaces is greatly minimized.[9,22,36] Other polarimetry techniques used for macular imaging have been used to improve the measurements of structures, such as the computation of retinal nerve fiber layer thickness that is based on the absolute retardance.[37–39]

Further improvement of polarimetry methods is being advanced by the use of Mueller matrix instrumentation, which completely specifies the polarization content in an image,[34,40–42] and by experiments to identify factors such as individual variations in anterior segment optics.[37,38,43] Both the specular and scattered light return, which were shown in panels B versus C in Figures 2 and 3 to provide different information for the optic nerve head structures, have been quantified with Mueller matrix polarimetry (Guthrie et al. *IOVS* 2004;45:ARVO Abstract 2796). Although the uses of polarimetry information are different, the mathematical treatments are closely related and well-described.[9,10,37,41,42]

Our sample included patients old enough to have aging changes to the cornea, lens, or vitreous that might alter the polarization results. None of the patients had severe enough changes to prevent color fundus photography, indicating that our sample did not include the most severe media changes. Two known artifacts of the cornea include an irregular tear film, which results in variation of optical power over the surface and over time, and individual differences in birefringence of the cornea.[37,38] When the corneal compensator does not correct for corneal birefringence, then our method overestimates somewhat the amount of depolarized light. This effect is generally constant across the retina. For example, 85% to 90% of the light returning from the normal retina retains polarization.[32] Therefore, if we remove only 70% of this component due to incomplete compensation of corneal birefringence, then the contrast of the depolarized light is two times higher. The addition of uniform depolarized light reduces image contrast to some extent. As for aging changes due to the lens, the polarization effects of the normal lens and most intraocular lenses are barely measurable with present instrumentation.[43] The effect of a cataractous lens has not been measured in detail with this instrumentation, except for the comparison of before versus after cataract extraction.[44] Such studies include not only the potential scattering of the cataractous lenses but also the alteration of corneal polarization due to wound healing after surgery. Differences on long-term follow-up were, on average, in the direction of improved signal amplitude with cataract extraction, but not generally statistically significant with either scanning laser polarimetry or confocal imaging. These findings are consistent with the idea that depolarization due to neither the cornea nor the lens has a large effect on the light return from the retinal plane, and consequently the computed depolarized image, due to the use of a confocal aperture to remove long-range scatter.

In a more general model, interesting polarization retaining information and possible artifacts could arise from sources not limited to the cornea—that is, when considering light return that is not limited to only birefringence or only the cornea and nerve fiber layer. The present method differs from the use of a static, cross-polarizer to remove glints that may occur in a given plane of polarization. Further, light collected at the detector for crossed polarization, regardless of the source, has no effect on the depolarized light image, as long as it is modulated in phase with the polarization preserving light that here is attributed to the nerve fiber layer, varying systematically according to the input polarization angle. Unlike the case of a single cross-polarized element, this modulating light is removed by the computation. Alternatively, any light reaching the detector for crossed polarization that does not modulate in phase with the light attributed to the nerve fiber layer serves to reduce the computed modulation and therefore reduces the contrast of the depolarized light images. The artifact is only in one direction— decreasing contrast—and does not add spurious features that are not present. The method described here clearly visualized the features of interest, some not otherwise visible, in a clinical population. Thus, further removal of artifacts, which although potentially small are inherent in an incomplete polarimetry device, would serve to make this method even better. Besides further reducing these already identified artifacts, the potential benefits of fully specifying polarization for pathologic structures is unknown in the eye. Image contrast in computed images as yet unavailable may be high for optically active molecules, and new information may be provided.

We tested only patients with clinically visible peripapillary hyperpigmentation, but we anticipate that this method may reveal similar findings in other patients with either more overlying nerve fiber layer, ocular pigmentation, or retinal disease such as epiretinal membrane that precludes visualization of hyperpigmentation. For patients undergoing scanning laser polarimetry in the management of glaucoma,[18,19,37–39] there is almost no additional time needed during patient data acquisition. As we did not experience difficulties in distinguishing fundus features, despite large atrophic regions prone to scatter, this method may be extended to peripapillary atrophy, known to be concordant with visual field loss.[45] This method may not only be more sensitive than traditional methods, but it also uses far less data storage. Thus, it should be considered for further studies for early detection of peripapillary changes improving the estimation of prognosis by factoring in peripapillary hyperpigmentation.

Acknowledgments

The authors thank the Ophthalmic Consultants of Boston for their continued assistance after the death of Ruthanne B. Simmons, MD; Michael C. Cheney, MS, for technical assistance; and Russell Chipman, PhD, for discussion of his model of computations from existing methods of scanning laser polarimetry.

References

1. Nicolela MD, McCormick BA, Drance OC, Ferrier MD, LeBlanc MD, Balwantray CC. Visual field and optic disc progression in patients with different types of optic disc damage: a longitudinal prospective study. *Ophthalmology*. 2003;110:2178–2184.
2. Primrose J. Early signs of the glaucomatous disc. *Br J Ophthalmol*. 1971;55:820–825.
3. Wilensky JT, Kolker AE. Peripapillary changes in glaucoma. *Am J Ophthalmol*. 1976;81:341–345.
4. Park KH, Park SJ, Lee YJ, Kim JY, Caprioli J. Ability of peripapillary atrophy parameters to differentiate normal-tension glaucoma from glaucomalike disk. *J Glaucoma*. 2001;10:95–101.
5. Jonas JB, Fernandez MC, Naumann GO. Parapapillary atrophy and retinal vessel diameter in nonglaucomatous optic nerve damage. *Invest Ophthalmol Vis Sci*. 1991;32:2942–2947.
6. Jonas. JB, Budde WM, Lang PJ. Parapapillary atrophy in the chronic open-angle glaucomas. *Graefes Arch Clin Exp Ophthalmol*. 1999; 237:793–799.
7. Buus DR, Anderson DR. Peripapillary crescents and halos in normal-tension glaucoma and ocular hypertension. *Ophthalmology*. 1989;96:16–19.
8. Sugiyama K, Tomita G, Kitazawa Y, Onda E, Shinohara H, Park KH. The associations of optic disc hemorrhage with retinal nerve fiber layer defect and peripapillary atrophy in normal-tension glaucoma. *Ophthalmology*. 1997;104:1926–1933.
9. Elsner AE, Miura M, Stewart JB, Kairala MBM, Burns SA. Novel algorithms for polarization imaging resulting in improved quantification of retinal blood vessels. *Stud Health Technol Inform*. 2003;94:59–61.
10. Burns SA, Elsner AE, Mellem-Kairala MB, Simmons RB. Improved contrast of subretinal structures using polarization analysis. *Invest Ophthalmol Vis Sci*. 2003;44:4061–4068.
11. Sarks JP, Sarks SH, Killingsworth MC. Evolution of geographic atrophy of the retinal pigment epithelium. *Eye*. 1988;2:552–577.
12. Curcio CA, Saunders PL, Younger PW, Malek G. Peripapillary chorioretinal atrophy: Bruch's membrane changes and photoreceptor loss. *Ophthalmology*. 2000;107:334–343.
13. Jonas JB, Fernandez MC, Naumann GOH. Glaucomatous parapapillary atrophy: occurrence and correlations. *Arch Ophthalmol*. 1992;110:214–222.
14. Elsner AE, Burns SA, Weiter JJ, Delori FC. Infrared imaging of sub-retinal structures in the human ocular fundus. *Vision Res*. 1996;36:191–205.
15. Kelley LM, Walker JP, Wing GL, Raskauskas PA, Elsner AE. Scanning laser ophthalmoscope imaging of age related macular degeneration and neoplasms. *J Ophthalmic Photogr*. 1997;3:89–94.
16. Elsner AE, Moraes L, Beausencourt E, et al. Scanning laser reflectometry of retinal and subretinal tissues. *Optics Express.* 2000;6: 243–250.

17. Elsner AE, Zhou Q, Beck F, et al. Detecting AMD with multiply scattered light tomography. *Int Ophthalmol*. 2001;23:245–250.
18. Weinreb RN, Dreher AW, Coleman A, Quigley H, Shaw B, Reiter K. Histopathologic validation of Fourier-ellipsometry measurements of retinal nerve fiber layer thickness. *Arch Ophthalmol*. 1990;108: 557–560.
19. Dreher AW, Tso PC, Weinreb RN. Reproducibility of topographic measurements of the normal and glaucomatous optic nerve head with the laser tomographic scanner. *Am J Ophthalmol*. 1991;111: 221–229.
20. Beausencourt E, Remky A, Elsner AE, Hartnett ME, Trempe CL. Infrared scanning laser tomography of macular cysts. *Ophthalmology*. 2000;107:375–385.
21. Elsner AE, Si YJ, Mellem-Kairala M, Miura M. Imaging and visualization of pathology beneath the retinal surface: medicine meets virtual reality. *Stud Health Technol Inform*. 2002;85:133–136.
22. Weber A, Cheney MC, Smithwick QYC, Elsner AE. Polarimetric imaging and blood vessel quantification. *Opt Express.* 2004;12: 5178–5190.
23. Weinreb RN, Dreher AW, Bille JF. Quantitative assessment of the optic nerve head with the laser tomographic scanner. *Int Ophthalmol*. 1989;13:25–29.
24. Burk RO, Volcker HE. Current imaging of the optic disk and retinal nerve fiber layer. *Curr Opin Ophthalmol*. 1996;7:99–108.
25. Ikram MK, van Leeuwen R, Vingerling JR, Hofman A, de Jong PT. Relationship between refraction and prevalent as well as incident age-related maculopathy: the Rotterdam Study. *Invest Ophthalmol Vis Sci*. 2003;44:3778–3782.
26. Fantes FE, Anderson DR. Clinical histologic correlation of human peripapillary anatomy. *Ophthalmology*. 1989;96:20–25.
27. Jonas JB, Nguyne XN, Gusek GC, Naumann GOH. The parapapillary chorio-retinal atrophy in normal and glaucoma eyes: I. Morphometric data. *Invest Ophthalmol Vis Sci*. 1989;30:908–918.
28. Jonas JB, Naumann GOH. Parapapillary chorio-retinal atrophy in normal and glaucoma eyes: II. Correlations. *Invest Ophthalmol Vis Sci*. 1989;30:919–926.
29. Klein R, Klein BE, Jensen SC, Meuer SM. The five-year incidence and progression of age-related maculopathy: the Beaver Dam Eye Study. *Ophthalmology*. 1997;104:7–21.
30. Klaver CC, Assink JJ, van Leeuwen R, et al. Incidence and progression rates of age-related maculopathy: *Invest Ophthalmol Vis Sci.* 2001;42:2237–2241.
31. Bressler SB, Maguire MG, Bressler NM, Fine SL. Relationship of drusen and abnormalities of the retinal pigment epithelium to the prognosis of neovascular macular degeneration. The Macular Photocoagulation Study Group. *Arch Ophthalmol*. 1990;108:1442–1447.
32. Blokland GJV, Norren DV. Intensity and polarization of light scattered at small angles from the human fovea. *Vision Res*. 1986;26: 485–494.
33. Elsner AE, Burns SA, Zhou Q, Dreher AW. Polarization modulation from in vivo human ocular fundus images. *Optics and Photonics News*. 1998;8:72.
34. Bueno JM, Campbell MCW. Confocal scanning laser ophthalmoscopy improvement by use of Mueller-matrix polarimetry. *Opt Lett*. 2002;27:830–832.
35. Cense B, Chen T, Park BH, Pierce MC, de Boer, JF. In vivo birefringence and thickness measurements of the human retinal nerve fiber layer using polarization-sensitive optical coherence tomography. *J Biomed Opt*. 2004;9:121–125.
36. Denninghoff KR, Smith MH, Lompado A, Hillman LW. Retinal venous oxygen saturation and cardiac output during controlled hemorrhage and resuscitation. *J Appl Physiol*. 2003;94:891–896.
37. Greenfield DS, Knighton RW, Feuer WJ, Schiffman JC, Zangwill L, Weinreb RN. Correction for corneal polarization axis improves the discriminating power of scanning laser polarimetry. *Am J Ophthalmol*. 2002;134:27–33.
38. Bagga H, Greenfield DS, Knighton RW. Scanning laser polarimetry with variable corneal compensation: identification and correction for corneal birefringence in eyes with macular disease. *Invest Ophthalmol Vis Sci*. 2003;44:1969–1976.
39. Weinreb RN, Zangwill L, Berry C, Bathija R, Sample P. Detection of glaucoma with scanning laser polarimetry. *Arch Ophthalmol*. 1998;116:1583–1589.
40. Prieto PM, Vargas-Martin F, McLellan JS, Burns SA. Effect of polarization on ocular wave aberration measurements. *J Opt Soc Am A*. 2002;19:809–814.
41. Chipman RA. Polarimetry. In: Bass M, van Stryland EW, Williams DR, Wolfe WI, eds. *The Handbook of Optics.* New York: McGraw Hill; 1994:1–27.
42. Bueno JM. Polarimetry in the human eye using an imaging linear polariscope. *J Opt A-Pure Appl Opt*. 2002;4:553–561.
43. Miura M, Osako M, Elsner AE, Kajizuka H, Uamada K, Usua M. Birefringence of intraocular lenses. *J Cataract Refract Surg*. 2004; 30:1549–1555.
44. Kremmer S, Garway-Heath DF, De Cilla S, Steuhl KP, Selbach JM. Influence of cataract surgery with implantation of different intraocular lenses on scanning laser tomography and polarimetry. *Am J Ophthalmol*. 2003;136:1016–1921.
45. Tezel G, Dorr D, Kolker AE, Wax MB, Kass MA. Concordance of parapapillary chorioretinal atrophy in ocular hypertension with visual field defects that accompany glaucoma development. *Ophthalmology*. 2000;107:1194–1199.